Available online at www.sciencedirect.com

SciVerse ScienceDirect

Ceramics International 39 (2013) 6631–6636

CERAMICS INTERNATIONAL

www.elsevier.com/locate/ceramint

Template assisted fabrication of TiO_2 and WO_3 nanotubes

Chien Chon Chen[a], Chin-Hua Cheng[b], Chung-Kwei Lin[c,*]

[a]Department of Energy Engineering, National United University, Miaoli 36003, Taiwan
[b]Department of Materials Science and Engineering, Feng Chia University, Taichung 40724, Taiwan
[c]School of Dental Technology, College of Oral Medicine, Taipei Medical University, Taipei 11031, Taiwan

Received 6 January 2013; received in revised form 28 January 2013; accepted 28 January 2013
Available online 8 February 2013

Abstract

Anodic aluminum oxide (AAO) templates with diameters of 200–500 nm were generated by anodizing a commercial aluminum (Al) substrate (99.7%) in 1 vol% phosphoric acid (H_3PO_4), with an applied voltage of 195 V. Titania and tungsten oxide nanotubes (NTs) were successfully grown on AAO template by the sol–gel process. Thermal gravimetric analyzer (TGA) curves showed that gel can be transfered to nanocrystalline particles after 19% weight loss of water molecule by evaporation. The results showed that the nanocrystalline TiO_2 NTs presented at 200 °C, and grains grew as temperature increased. At a temperature of 550 °C, the (101), (103), (004), (112), (200), (105), and (211) planes of anatase TiO_2 were detected clearly, whereas tungsten oxide NTs are amorphous after heat treatment at 200 °C or 300 °C. But the (110), (111), (002), (022), (222), and (004) planes of γ-WO_3 phase can be observed obviously after the heat treatment at 400 °C.

Keywords: A. Sol–gel; Titania; Tungsten oxide; Nanotube; AAO

1. Introduction

Many nanostructures have very interesting properties. For example, titania has been used in various applications such as environment [1], catalysis [2], dielectrics [3], optoelectronics [4], sensors [5], and solar cells [6–8]. Also, WO_3 nanopores show excellent ion intercalation properties (electrochromic devices, charge storage) [9–13]. The oxides have varied stable phases. For example, titanium dioxide has three stable phases: anatase, brookite, and rutile [14]. Tungsten oxide has four: α-WO_3 (tetragonal, 1010–1170 °C), β-WO_3 (orthorhombic, 600–1170 °C), γ-WO_3 (monoclinic, 290–600 °C), and δ-WO_3 (triclinic, 230–290 °C) [15]. The transformation of those phases depends on the annealing temperature at a constant oxygen pressure, as in an air furnace.

It is also interesting that in the case of titanium alloys, small amounts of the alloying element can drastically affect the properties, while the unique nano-tubular morphology is completely retained. For example, TiW (0.2 at%) alloys show a strongly enhanced electrochromic response and improved photocatalytic properties [16]. Yang et al. [17] doped WO_3 into TiO_2 NT to enhance the photo-catalysis property. Smith and Zhao [18] produced a TiO_2/WO_3 core/shell structure that enhances the separation rate of electrons and holes. Xiao et al. [19] coated WO_3 particles on TiO_2 NT; this nano-composite material can reduce the recombination rate of electrons and holes. Schmuki made TiO_2–WO_3 composite nanotubes by TiW alloy anodization; such nanotubes have an excellent dye-absorbance ability [20].

AAO has characteristics of being light and transparent, with large surface, good mechanical strength, and flexibility, making it a candidate material for the template. In this work, AAO template was made by anodization; TiO_2 and WO_3 NTs were made by the sol–gel deposition on AAO. We also examined the morphology and crystallization characteristics in the above nano-materials. The effects of post heat-treatment on the morphology and phase transformation of TiO_2 NT and WO_3 NT were examined by SEM, TEM, EDS, XRD, XAS, XPS, TGA, and FTIR analysis.

*Corresponding author. Tel.: +8862 2736 1661x5115.
E-mail address: chungkwei@tmu.edu.tw (C.-K. Lin).

0272-8842/$ - see front matter © 2013 Elsevier Ltd and Techna Group S.r.l. All rights reserved.
http://dx.doi.org/10.1016/j.ceramint.2013.01.100

2. Experimental procedures

2.1. AAO template fabrication

Anodic aluminum oxide (AAO, Al_2O_3) templates with a pore size of 10–500 nm were generated by a two-step anodizing process on a commercial aluminum (Al) substrate (99.7%) in acid solutions of sulfuric acid (H_2SO_4), oxalic acid $(COOH)_2$, or phosphoric acid (H_3PO_4). The Al substrate was first ground to # 1000 by SiC waterproof paper. Then the residual stress of the Al substrate was released by annealing at 550 °C for 1 h in an air furnace. After annealing, the sample was electro-polished in a bath consisting of 15 vol% perchloric acid ($HClO_4$, 70%), 70 vol% ethanol (C_2H_6O, 99.5%), and 15 vol% monobutylether ($(CH_3(CH_2)_3OCH_2CH_2OH$), 85%) with 42 V (DC) applied for 10 min and titanium foil used as a counter. AAO templates with diameters of 200–500 nm were generated by anodizing a commercial aluminum (Al) substrate (99.7%) in 1 vol% phosphoric acid (H_3PO_4), with applied voltages of 195 V and pore widening using 5 vol% H_3PO_4 for 0.5–4 h. A more detailed description of the AAO process can be found in our previous study [21–23].

2.2. TiO_2 NT formation in AAO

The TiO_2 NT was prepared by immersing the Al_2O_3 template in 0.02 M titanium fluoride (TiF_4) solution. The immersion steps were as follows: (1) adjust pH value of DI-water to 1.0–1.3 using hydrochloric acid (HCl); (2) add TiF_4 into DI-water; (3) immerse sample into TiF_4 solution for 10 min; (4) adjust pH value of TiF_4 solution to 3.0–3.3 using NH_4OH (ammonium hydroxide); and (5) immerse sample into TiF_4 solution for 120 min. After the immersion steps, the sample was annealed at 200, 300, 400, and 550 °C for 1–3 h to obtain anatase TiO_2 NT on the Al_2O_3 template.

2.3. WO_3 NT formation in AAO

The WO_3 NT was prepared by immersing Al_2O_3 template into tungsten (VI) chloride (WCl_6) containing sol–gel as follows: (1) make tungsten precursor in ethanol (C_2H_5OH) solvent with 10 wt% WCl_6 and 2 h stirring; (2) add 20 vol% surface-active agent of 2,4-pentanedione ($C_5H_8O_2$) to the solution with 2 h stirring again to form tungsten-containing sol; (3) add 0.15 vol% DI-water to the solution with 12 h stirring to form tungsten-containing sol–gel; (4) immerse sample in tungsten (VI) chloride (WCl_6) containing sol–gel for 1 h and (5) after the immersion steps, the sample was annealed at 550 °C for 1 h to obtain γ-phase (monoclinic) WO_3 NT on the Al_2O_3 template.

2.4. TiO_2/WO_3 NTs formation in AAO

The TiO_2 NT was first formed on the AAO template by TiF_4 solution, and then the sample was immersed in 10 wt% sodium tungstate dihydrate ($Na_2WO_4 \cdot 2H_2O$)

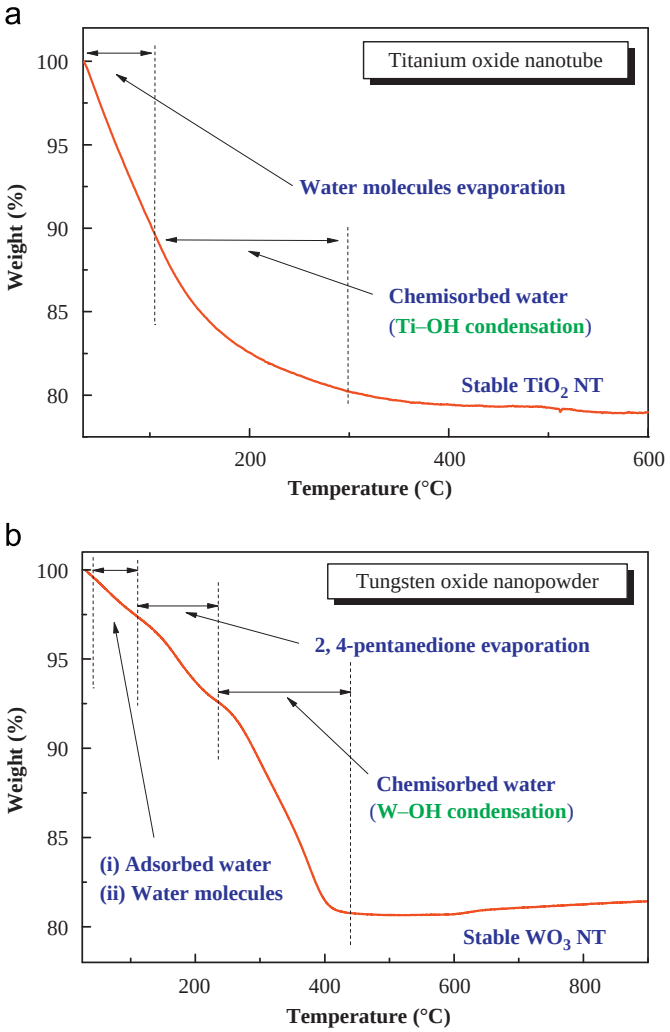

Fig. 1. TGA curves of (a) TiO_2 NT between 25 and 600 °C and (b) WO_3 NT between 25 and 900 °C.

Table 1
Summary of the experimental procedures of methods, solution, and heat treatment temperature.

Materials	Fabrication method	Crystallization
AAO	1 vol% H_3PO_4, 195 V anodization and 5 vol% H_3PO_4 pore widening for 0.5–4 h	Amorphous
TiO_2 NT	Sol–gel: 0.02 M TiF_4 (pH:3.0–3.3) for 2 h	550 °C for anatase phase
WO_3 NT	Sol–gel: 10 wt% WCl_6,20 vol% $C_5H_8O_2$ and 15 vol% C_2H_5OH for 17 h	400 °C for γ-phase

solution for 1 h to form TiO_2/WO_3 NTs in AAO. The experimental procedures are summarized in Table 1.

2.5. TiO_2 and WO_3 NT images

Because of the robust structure of the NT and the loose structure of the surface debris, the unwanted deposits on the AAO surface introduced during the sol–gel process can be effectively removed with ultrasonic vibration of the AAO in deionized water. Free-standing NTs were collected after the AAO template was dissolved thoroughly in 0.4 M phosphoric acid (H_3PO_4)+0.2 M chromium (CrO_3) mixture solution at ~60 °C for 1 h. After sonication the supernatant was carefully removed with syringe and replaced with de-ionized water. This was repeated several times to rinse the NTs. For the final step, the de-ionized water was replaced by isopropanol and after dispersing the NTs by sonication, a drop of the isopropanol–NTs suspension was deposited onto Cu grid with carbon film for TEM observation.

The micro-morphology and composition of NTs were determined by scanning electron microscopy (SEM, JEOL 6500), transmission electron microscopy (TEM, JEOL 2100F), X-ray diffraction (XRD, PHILIPS X'Pert Pro), Fourier transform infrared spectroscopy (FTIR), and thermal gravimetric analysis (TGA 2950, TA Instrument).

3. Results and discussion

3.1. TiO_2 and WO_3 NT crystallization

Because TiO_2 NTs were formed in the AAO by sol–gel process, the retained solvent had to be removed by heat treatment. In order to understand the details of the heat treatment condition, the TGA test was used for TiO_2 NT. Fig. 1 shows the TGA curves of (a) TiO_2 NT and (b) WO_3

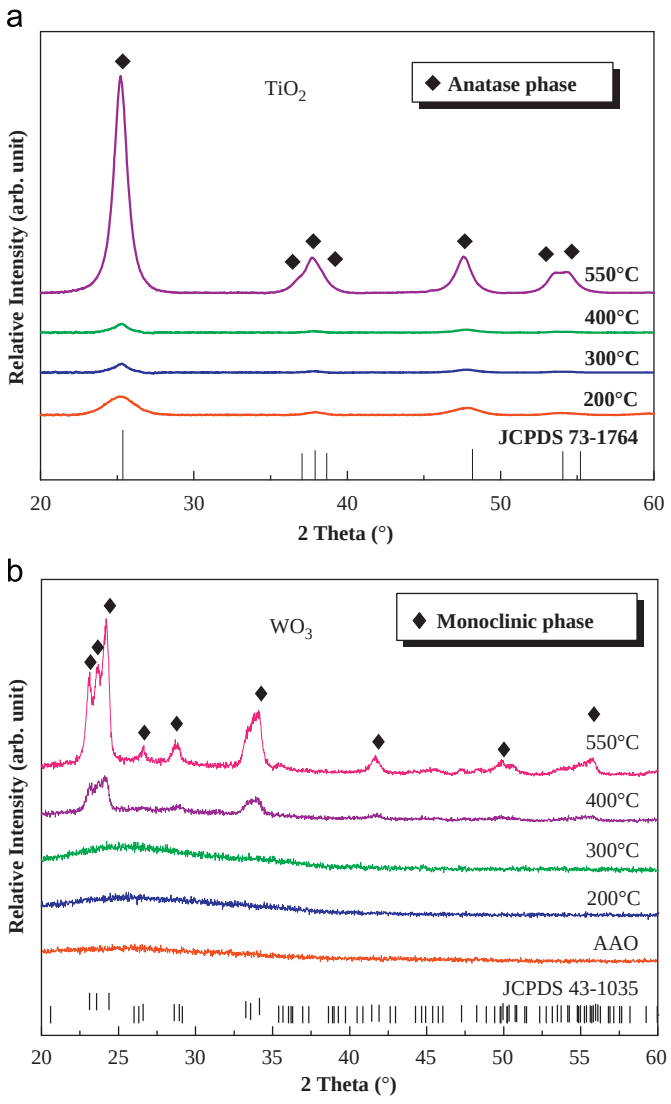

Fig. 2. XRD patterns of (a) TiO_2 NT and (b) WO_3 NT deposited inside amorphous AAO templates by the sol–gel method.

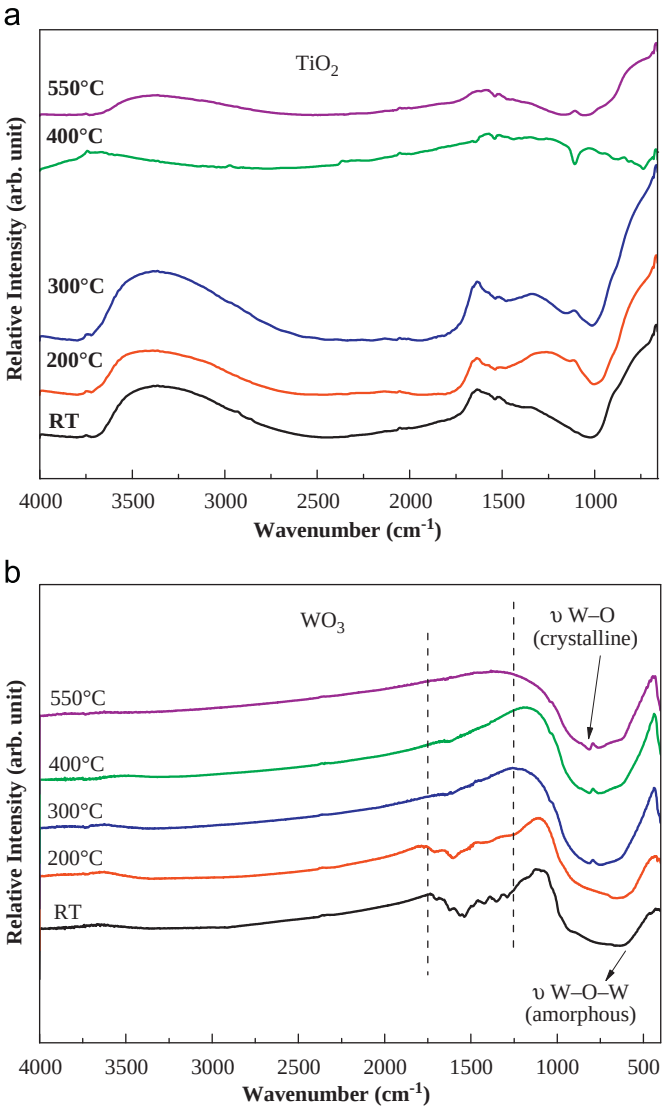

Fig. 3. FTIR patterns of (a) TiO_2 NT and (b) WO_3 NT deposited inside AAO templates by the sol–gel method.

NT on the AAO from 25 to 600 °C and 25 to 900 °C with a heating rate of 5 °C/min. The TGA curve of TiO_2 NT shows obvious weight loss regions: (1) a 19% weight loss region due to water molecule evaporation, ($Ti(OH)_{4-x}F_x$ is transformed to $Ti(OH)_4$), and chemisorbed water ($Ti(OH)_4$ (25–300 °C), and (2) a stable TiO_2 NT region (above 300 °C). Therefore, the sol–gel TiO_2 NT can be stabilized with heat treatment at 300 °C for 1 h. The TGA curve of WO_3 NT shows obvious weight loss regions: (1) a 19% weight loss region due to water molecule evaporation, 2, 4-pentanedione evaporation, and $W(OC_2H_5)_6$ condensing to WO_3 (25–420 °C) [24], and (2) a stable WO_3 NT region (above 420 °C). Therefore, the sol–gel WO_3 NT can be stabilized with 1 h heat treatment at 420 °C.

The crystallizations of TiO_2 NT and that of WO_3 NT were tested by heat treatment and XRD process. Fig. 2(a) shows XRD patterns of TiO_2 NT inside the amorphous AAO template produced by sol–gel method with heat treatments varied from 200 to 550 °C for 1 h. With temperatures at 200, 300, and 400 °C, the peaks were present at 2θ values of 25.3°, 37.9°, and 48.1°,respectively, and the full width at half maximum decreased as heat treatment temperature increased. Therefore, the nano-crystalline TiO_2 presented at 200 °C, and grains grew as temperature increased. At a temperature of 550 °C, the obvious diffraction peaks at 25.3°, 37.0°, 37.9°, 38.6°, 48.1°, 54.0°, and 55.2°, corresponding to the (101), (103), (004), (112), (200), (105), and (211) planes of anatase TiO_2 were detected. In order to eliminate the effect of AAO, AAO was dissolved in a 1 M NaOH aqueous solution, and pure TiO_2 NT was obtained. Fig. 2(b) shows XRD patterns of WO_3 NT grown on the amorphous AAO template by the sol–gel method after heat treatment for 1 h at 200–550 °C with sintering at 200 and 300 °C. The WO_3 NTs were amorphous, and after sintering at 400°C, the peaks were present at 2θ values of 22.5–25° and 32.5–35°. At 550 °C, the obvious diffraction peaks of 23.1°, 23.5°, and 24.2°, corresponding to γ-WO_3 were detected. The crystallizations of TiO_2 NT and that of WO_3 NT were further tested by heat treatment and FTIR. Fig. 3 shows FTIR spectra of pure (a) TiO_2 NT and (b) WO_3 NT after heat treatments at various temperatures. For the TiO_2 NT curve, the peaks showed the Ti–OH bonding vibration of $Ti(OH)_4$ (1625 cm^{-1}) under 200 and 300 °C, the –OH bonding vibration in water molecules (3000–3500 cm^{-1}) below 300 °C, and the Ti–O bonding vibration (wave number less than 1000 cm^{-1}) at RT, 200, 300, 400, and 550 °C. For the TiO_2 NT curve, the peaks showed the $C_5H_8O_2$ bonding vibration (1200–1750 cm^{-1}) at RT and 200 °C, and the crystalline bonding vibration (717 and 810 cm^{-1}) at 300, 400, and 550 °C.

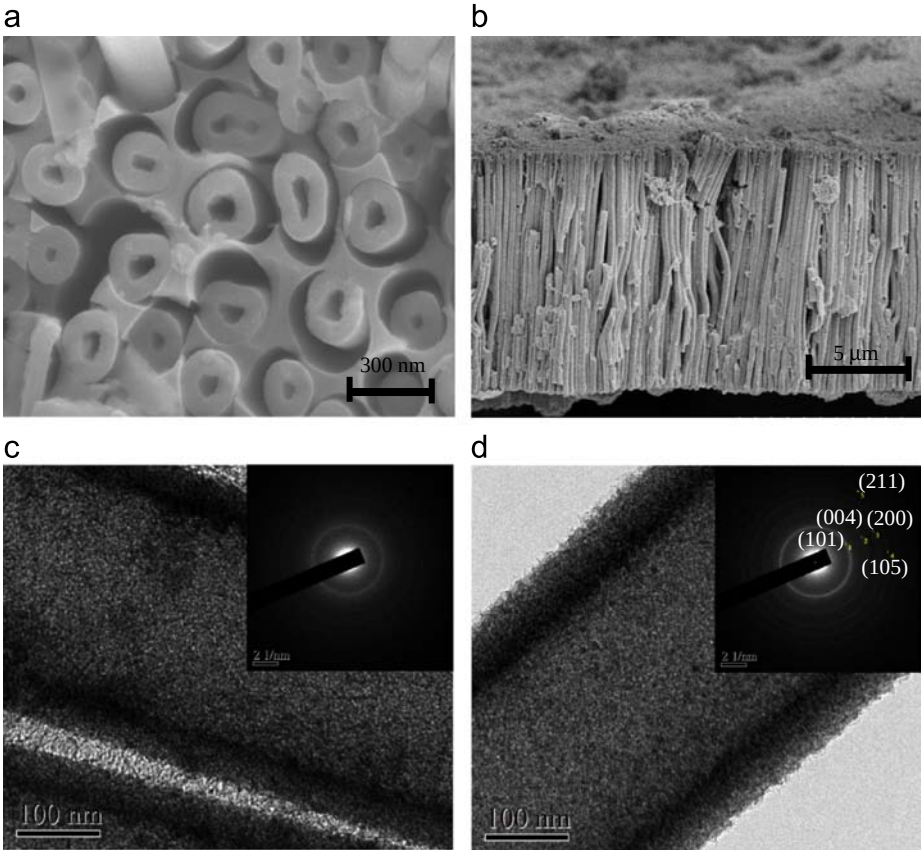

Fig. 4. SEM images of TiO_2 NT on AAO template; (a) top view and (b) side view. TEM images and electron diffraction (ED) patterns of TiO_2 NT after (c) 400 °C and (d) 550 °C annealing; with higher annealing temperature, more complete crystallization of TiO_2 NT was observed.

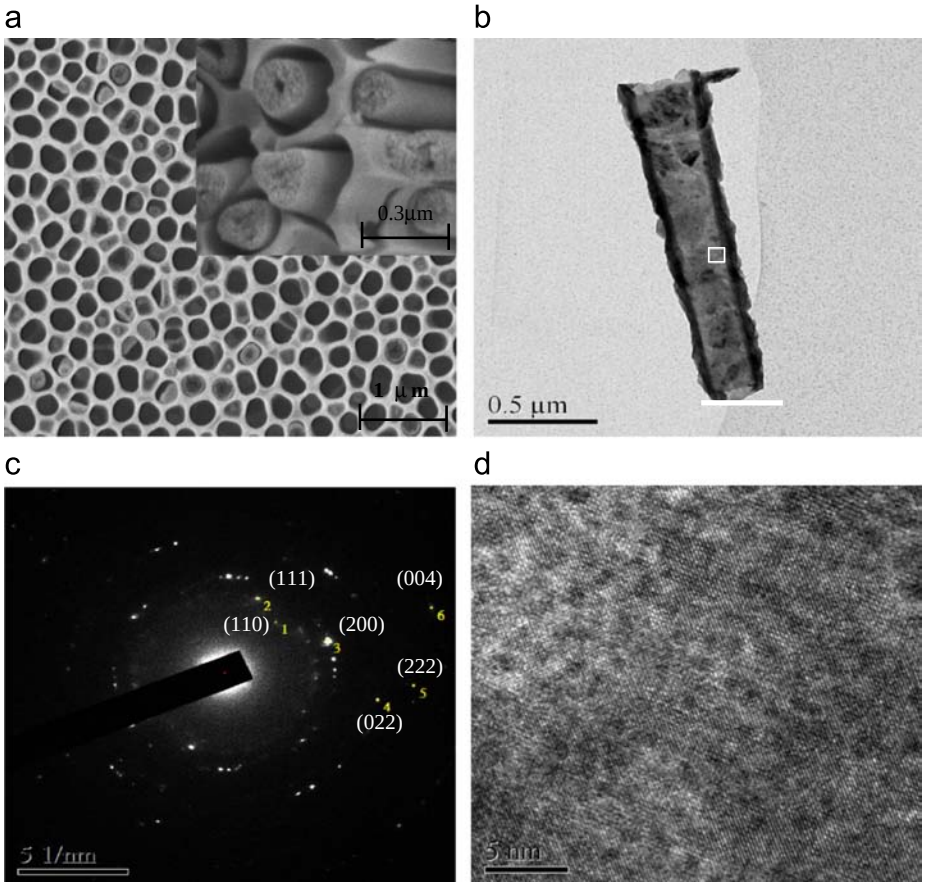

Fig. 5. (a) SEM images of WO_3 NT on the AAO template, (b) TEM image of WO_3 NT with 400 nm pore diameter, (c) polycrystalline SAE image, and (d) HRTEM image of WO_3 NT.

3.2. TiO_2 and WO_3 NT images

Fig. 4 shows images of TiO_2 NT on the AAO template: (a) top view of TiO_2 NT with 100–200 nm pore size and 50–80 nm pore wall on the AAO template with 200–350 nm pore diameters; and (b) side view of TiO_2 NTs of 13 μm standing on AAO template. According to the SEM images, there was no metallurgical interface between the TiO_2 NT and AAO template; therefore, the TiO_2 NTs could be collected when the AAO template was dissolved by a chemical solution such as base solution. Fig. 4(c) and (d) shows TEM images of TiO_2 NT after annealing at 400, and 550 °C. The images show that TiO_2 NT had a pore wall thickness of 50–80 nm and a pore diameter of 100–200 nm, depending on the AAO pore size. TiO_2 NT diffraction (ED) patterns also showed that the first diffraction ring appeared and the *d*-space was 3.50 Å. The intensity of the first diffraction ring increased with increasing heat treatment temperature. Comparing the first diffraction ring to Fig. 2 XRD patterns, the first diffraction ring is in the (101) plane. At 550 °C, obvious diffraction rings could be observed, indicating polycrystalline TiO_2 NT.

Based on the analyses of TiO_2 NT on the AAO template, we also grew the WO_3 NT on the AAO template by the sol–gel process. Fig. 5 shows WO_3 NT images; (a) SEM images of WO_3 NT on the AAO template, (b) TEM images of WO_3 NT after 550 °C annealing with 400 nm pore diameter, (c) polycrystallinity of SAE image with *d*-space values of 2.85, 2.42, 1.99, 1.40, 1.16, and 0.99 Å, corresponding, respectively, to the (110), (111), (002), (022), (222), and (004) planes of monoclinic WO_3 (γ-WO_3) phase, and (d) an HRTEM image also showing crystallization of WO_3 NT.

4. Conclusions

Titania nanotubes and tungsten oxide nanotubes have been prepared by AAO template assistance and the sol–gel method. TiO_2 with anatase phase and WO_3 with monoclinic phase were achieved through 550 °C heat treatment of gel-type TiO_2 and WO_3. During annealing of TiO_2 NT, three obvious weight loss regions—the water molecule evaporation region (25–100 °C), chemisorbed water and removal of F atoms region (100–300 °C), and stable TiO_2 NT (above 300 °C)—presented. During annealing of WO_3 NT, four obvious weight loss regions—water molecule evaporation region (25–100 °C), 2,4-pentanedione evaporation (100–220 °C), chemisorbed water evaporation (220–420 °C), and stable WO_3 NT (above 420 °C)—presented.

Acknowledgments

The authors would like to thank the National Science Council of Taiwan (101-2627-M-239-001), Feng Chia University, and National United University for financial support to this work. The authors also thank the entire staff at NSRRC (Hsinchu, Taiwan, ROC) for their expert assistance.

References

[1] M. Raimondo, G. Guarini, C. Zanelli, F. Marani, L. Fossa, M. Dondi, Printing nano TiO_2 on large-sized building materials: technologies, surface modifications and functional behaviour, Ceramics International 38 (2012) 4685–4693.
[2] S. Ramya, S.D. Ruth Nithila, R.P. George, D. Nanda Gopala Krishna, C. Thinaharan, U. Kamachi Mudali, Antibacterial studies on Eu–Ag codoped TiO_2 surfaces, Ceramics International 39 (2013) 1695–1705.
[3] L. Snashall, Lasse Norén, Yun Liu, Toru Yamashita, Frank Brink, L. Withers, Phase analysis and microwave dielectric properties of $BaO–Nd_2O_3–5TiO_2$ composite ceramics using variable size TiO_2 reagents, Ceramics International 38 (2012) S153–S157.
[4] Z. Tun, J.J. Noel, D.W. Shoesmith, Electrochemical modification of the passive oxide layer on a Ti film observed by in-situ neutron reflectometry, Journal of the Electrochemical Society 146 (1999) 988.
[5] O.K. Varghese, G.K. Mor, C.A. Grimes, M. Paulose, N. Mukherjee, A titania nanotube-array room-temperature sensor for selective detection of hydrogen at low concentrations, Journal of Nanoscience and Nanotechnology 4 (2004) 733–737.
[6] C.C. Chen, S.J. Hsieh, Evaluation of fluorine ion concentration in titanium oxide nanotube (TiO_2 NT) anodization process, Journal of the Electrochemical Society 156 (2010) K125–K130.
[7] H.P. Wu, L.L. Li, C.C. Chen, W.G. Diau, Anodic TiO_2 nanotube arrays for dye-sensitized solar cells characterized by electrochemical impedance spectroscopy, Ceramics International 38 (2012) 6253–6266.
[8] C.C. Chen, W.D. Jehng, L.L. Li, W.G. Diau, Enhanced efficiency of dye-sensitized solar cells (DSSC) using anodic titanium oxide (ATO) nanotube arrays, Journal of the Electrochemical Society 156 (2009) C304–C312.
[9] W.D. Jheng, Logotype-selective electrochromic glass display, Ceramics International 38 (2012) 5835–5842.
[10] S. Reich, G. Leitus, Y. Tssaba, Y. Levi, A. Sharoni, O. Millo, Localized high-T_c superconductivity on the surface of Na-doped WO_3, Journal of Superconductivity 13 (2000) 855–861.
[11] C.C. Chen, Characterization of porous WO_3 electrochromic device by electrochemical impedance spectroscopy, Journal of Nanomaterials, Accepted for publication.
[12] X. Zhao, T.L.Y. Cheung, X. Zhang, D.H.L. Ng, J. Yu, Facile preparation of strontium tungstate and tungsten trioxide hollow spheres, Journal of the American Ceramic Society 89 (2006) 2960–2963.
[13] D. Garg, P.B. Henderson, R.E. Hollingsworth, D.G. Jensen, An economic analysis of the deposition of electrochromic WO_3 via sputtering or plasma enhanced chemical vapor deposition, Materials Science and Engineering B 119 (2005) 224–231.
[14] P.M. Woodward, A.W. Sleight, T. Vogt, Ferroelectric tungsten trioxide, Journal of Solution Chemistry 131 (1997) 9–17.
[15] Marcel Pourbaix, Atlas of Electrochemical Equilibria in Aqueous Solution, NACE, USA 213, 1974.
[16] Y.C. Nah, A. Ghicov, D. Kim, S. Berger, P. Schmuki, $TiO_2–WO_3$ composite nanotubes by alloy anodization: growth and enhanced electrochromic properties, Journal of the American Chemical Society 130 (2008) 16154–16155.
[17] L. Yang, Y. Xiao, S. Liu, Y. Li, Q. Cai, S. Luo, Photocatalytic reduction of Cr (VI) on WO_3 doped long TiO_2 nanotube arrays in the presence of citric acid, Applied Catalysis B 94 (2010) 142–149.
[18] W. Smith, Y.P. Zhao, Catal. Commun., Superior photocatalytic performance by vertically aligned core–shell TiO_2/WO_3 nanorod arrays, Catalysis Communications 10 (2009) 1117–1121.
[19] M.W. Xiao, L.S. Wang, X.J. Huang, Y.D. Wu, Z. Dang, Synthesis and characterization of WO_3/titanate nanotubes nanocomposite with enhanced photocatalytic properties, Journal of Alloys and Compounds 470 (2009) 486–491.
[20] Y.C. Nah, A. Ghicov, D. Kim, S. Berger, P. Schmuki, $TiO_2–WO_3$ composite nanotubes by alloy anodization: growth and enhanced electrochromic properties, Journal of the American Chemical Society 130 (2008) 16154–16155.
[21] C.C. Chen, D. Fang, Z. Luo, Fabrication and characterization of highly-ordered valve-metal oxide nanotubes and their derivative nanostructures: a review, Reviews in Nanoscience and Nanotechnology 1 (2012) 229–256.
[22] C.C. Chen, C.L. Chen, Y.S. Lai, Template assisted fabrication of Pt–Sn core–shell nanospheres, Materials Chemistry and Physics 131 (2011) 250–253.
[23] K.H. Yang, C.C. Chen, Alumina template assistance in titania nanotubes dye-sensitized solar cell (TiO_2 NT-DSSC) device fabrication, ISRN Nanotechnology Article ID 132797 (2012) 10 p.
[24] K. Nishio, T. Set, T. Tsuchiya, Preparation of electrochromic tungsten oxide thin film by sol–gel process, Journal of the Ceramic Society of Japan. 107 (1999) 199–203.